RSC Advances

PAPER

View Article Online
View Journal | View Issue

Cite this: *RSC Adv.*, 2026, **16**, 11208

Enhancing prebiotic production by engineering the levanbiose-binding site of *Erwinia tasmaniensis* levansucrase

Thanapon Charoenwongpaiboon,[a]* Yanisa Srichompoo,[a] Wannarat Chanket,[a] Stefano Benini,[b] Robert A. Field,[c] Chanchao Lorthongpanich,[d] Piamsook Pongsawasdi,[e] Peerapon Deetanya,[f] Rath Pichyangkura[e] and Karan Wangpaiboon[f]

Received 29th December 2025
Accepted 12th February 2026

DOI: 10.1039/d5ra10086k

rsc.li/rsc-advances

Levan-type fructooligosaccharides (LFOSs) possess valuable bioactivities but are produced in low yields by Gram-negative bacterial levansucrases. Here, we rationally engineered the levanbiose-binding site of *Erwinia tasmaniensis* levansucrase (*Et*Lsc) to enhance LFOS synthesis. Eleven residues surrounding the levanbiose-binding site were substituted to disrupt levan chain binding or to modulate loop flexibility. The results indicate that D82A, R377A, and G379P do not synthesize levan polymers. In addition, R377A and G379P largely produced LFOS, converting 35% and 24% of sucrose into LFOS. Affinity PAGE confirmed the loss of the levan-binding ability of the R377A and G379P variants. MD simulations revealed that G379P induces a structural rearrangement of loop II, altering the orientation of the key residue R377. Prebiotic activity analysis demonstrated that LFOS synthesized by the R377A variant stimulated the growth of probiotic bacteria, including *Limosilactobacillus fermentum*, and *Lacticaseibacillus casei*, more effectively than inulin. Together, these results identify R377 and G379 as critical determinants of levan elongation and demonstrate a promising strategy for enhancing LFOS production with Gram-negative levansucrases.

1. Introduction

Fructooligosaccharides (FOS) are well-known prebiotics, widely used as supplements in food and feed products. They have been reported to have potential for modulating immune responses, reducing serum cholesterol levels, enhancing mineral absorption, and stimulating the growth of beneficial gut microbiota.[1–3] In addition, FOS serve as non-caloric sweeteners, making them particularly suitable for individuals with diabetes.[4] Based on their glycosidic linkages, FOS can be classified into two major groups: inulin-type fructooligosaccharides (IFOSs), which comprise linear β-2,1-linked fructans, and levan-type fructooligosaccharides (LFOSs), where fructose residues are connected by β-2,6 linkages in the main chain and a β-2,1 linkage in the side chains.

Generally, IFOSs are synthesized from sucrose using β-fructofuranosidase (E.C. 3.2.1.26) or inulosucrase (E.C. 2.4.1.9).[5] IFOSs are common oligosaccharides and are widely available commercially. In contrast, LFOSs are classified as rare sugars and can be produced from sucrose only through the activity of levansucrase (E.C. 2.4.1.10). Previous studies have reported that LFOSs and levan selectively stimulate the growth of beneficial gut microbiota. In addition, they exhibit several bioactive properties, including anti-oxidative, anti-inflammatory, and anti-cancer.[6,7]

The molecular weight of levan influences its biological functions. Shorter levan chains often demonstrate enhanced biological activity compared to high-molecular-weight levan, mostly owing to their higher bioavailability.[6] Several strategies have been employed to increase the yield of low-molecular-weight levan and LFOS. Partial hydrolysis of levan with endo-levanase can produce LFOSs with varying degrees of polymerization (DP). Levansucrase and endo-levanase can also be fused into a single enzyme molecule or co-immobilized to enable one-pot LFOS synthesis.[8,9] Furthermore, supplementing levansucrase reactions with 1-kestose or inulosucrase can suppress polymerization activity and thereby increase the LFOS yield.[10]

[a]*Department of Chemistry, Faculty of Science, Silpakorn University, Nakhon Pathom 73000, Thailand. E-mail: charoenwongpaib_t@su.ac.th*

[b]*Bioorganic Chemistry and Bio-Crystallography laboratory (B_2Cl), Faculty of Agricultural, Environmental and Food Sciences, Free University of Bolzano, Piazza Università 5, 39100 Bolzano, Italy*

[c]*School of Chemistry, Pharmacy and pharmacology, University of East Anglia, Norwich Research Park, Norwich, NR4 7TJ, UK*

[d]*Siriraj Center of Excellence for Stem Cell Research, Faculty of Medicine Siriraj Hospital, Mahidol University, Bangkok, Thailand*

[e]*Department of Biochemistry, Faculty of Science, Chulalongkorn University, Bangkok 10330, Thailand*

[f]*Center of Excellence in Structural and Computational Biology, Department of Biochemistry, Faculty of Science, Chulalongkorn University, Bangkok 10330, Thailand*

Enzyme engineering represents another approach that has been used to alter the degree of polymerization of the oligosaccharides produced by glycoside transferases. This approach typically involves mutating amino acid residues within the acceptor-binding site to reduce interactions with potential acceptor oligosaccharide chains. Therefore, understanding the structure–function relationship of the enzyme is essential for successful application of this strategy. For levansucrase, enzyme engineering in order to modulate product size and enhance LFOS yield has been highly successful, particularly for Gram-positive bacterial enzymes. For instance, the use of computational design to control the chain length of LFOS generated by levansucrase from *Bacillus licheniformis* at DP 5 (ref. 11) and the rational design of levansucrase from *Bacillus amyloliquefaciens* to increase the yield of LFOS.[12] In contrast, attempts to improve LFOS production from Gram-negative bacterial levansucrases through protein engineering have been less successful. For instance, the A197D and F198N mutations in *Erwinia amylovora* levansucrase reduced the formation of high-molecular-weight levan but did not substantially increase LFOS yield.[13] This limited progress was likely due to an incomplete understanding of the polymer extension mechanism of Gram-negative levansucrases at the time.

Recently, the levan extension mechanism of *Erwinia tasmaniensis* levansucrase (*Et*Lsc) was explained by extensive mutagenesis analysis. The results revealed that *Et*Lsc possesses a distinct levan-binding track compared to that of *Bacillus* enzymes.[14] Furthermore, the direction of this track was found to point toward the levanbiose-binding region reported in the crystal structure.[15] This levanbiose-binding region is located on a flexible loop, whose conformations change upon levan binding. Herein, rational mutation at residues within the levanbiose-binding site of *Et*Lsc was performed with the expectation of enhancing LFOS synthesis. The residues to be mutated were selected based on the orientation of their side chains, and specifically those likely to interact with the levan acceptor. In addition, glycine residues within this region were replaced with proline to reduce loop flexibility. These studies provide new insights with the potential to enhance the applicability of Gram-negative levansucrases in the production of bioactive oligosaccharides.

2. Experimental

2.1 Site-directed mutagenesis

Variant *Et*Lsc plasmids were constructed using the same methods as described previously.[14] In brief, the variant gene was constructed using the PCR overlapping extension method.[16] The oligonucleotide primers used in this study are listed in Table S1. Gene amplification was performed using PrimeSTAR HS DNA Polymerase (Takara Bio) under the following conditions: initial denaturation at 98 °C for 2 min, followed by 25 cycles of denaturation at 98 °C for 10 s, annealing at 55 °C for 10 s, and extension at 72 °C for 1 min 30 s, with a final extension at 72 °C for 3 min. The resulting PCR products were separated by agarose gel electrophoresis and purified using a GenepHlow™ Gel/PCR Kit (Geneaid). The purified variant genes were cloned into the pMCSG49 vector *via* the *Nde*I and *Xho*I restriction sites and subsequently transformed into *Escherichia coli* Top10 for propagation.

2.2 Protein expression and purification

The sequence-verified plasmids were transformed into *E. coli* BL21 (DE3). The transformants were spread onto LB agar plates supplemented with 0.1 mg mL^{-1} ampicillin and incubated at 37 °C for 16–18 h. Several colonies were picked and inoculated into 20 mL of LB broth containing 0.1 mg mL^{-1} ampicillin, followed by incubation at 37 °C with shaking for 16–18 h. The resulting starter culture was transferred into fresh LB broth supplemented with 0.1 mg mL^{-1} ampicillin and 5 g L^{-1} glucose at a 1 : 100 inoculation ratio. The culture was grown at 37 °C and 200 rpm until the OD600 reached 0.4–0.6. Protein expression was then induced by adding 0.5 mM IPTG, and the culture was further incubated at 20 °C and 200 rpm for 16–18 h. The cells were harvested by centrifugation at 8000 × *g* for 10 min, resuspended in 25 mM potassium phosphate buffer (pH 7.4), and lysed by ultrasonication. The crude enzyme was purified using a TOYOPEARL™ AF-Chelate 650 M column as described in the previous study.[14] In brief, the crude extract protein was applied to the column preequilibrated with 25 mM potassium phosphate buffer. The column was washed with the same buffer supplemented with 20 mM imidazole and 200 mM NaCl. Finally, the target proteins were eluted using buffer containing 200 mM imidazole at pH 7.4.

2.3 Activity assay

The enzyme activity was determined using the dinitrosalicylic acid (DNS) method[17] and glucose oxidase methods as previously described.[14] The purified enzyme was incubated with 0.5 mL of 500 mM sucrose in 50 mM potassium phosphate buffer (pH 7.4) at 37 °C. After that, reactions were stopped by adding 20 μL of 1 M NaOH. Total reducing sugars (glucose + fructose) were determined by the DNS assay, whereas the glucose concentration was quantified by the glucose liquicolor kit (HUMAN™). For the DNS assay, 0.5 mL of DNS reagent was added to 0.5 mL of reaction mixture, followed by boiling for 10 min. The concentration of reducing sugars was determined from a calibration curve based on absorbance at 540 nm. Glucose concentration was determined by mixing 5 μL of the reaction mixture with 250 μL of glucose liquicolor reagent in a microplate, followed by incubation at room temperature for 15 min and measurement of absorbance at 500 nm. The fructose concentration was determined by subtracting glucose from the overall reducing sugar concentration. One unit of enzyme activity is defined as the quantity of enzyme that liberates 1 μmol of glucose per minute under the specified assay conditions.

2.4 Enzyme kinetic

Kinetic parameters were determined by analysing enzyme activity as a function of sucrose concentration. Reactions were performed using sucrose concentrations from 0 to 640 mM in 50 mM potassium phosphate buffer (pH 6.5) at 37 °C. The total

catalytic activity (V^G) of *Et*Lsc was defined as the rate of glucose formation, whereas the hydrolytic activity (V^F) corresponded to the rate of fructose production. The transfructosylation activity (V^{G-F}) was obtained by subtracting V^F from V^G. The resulting activity–substrate concentration data were fitted to either the Michaelis–Menten or substrate inhibition model to derive kinetic parameters (see SI, Fig S1 for details).

2.5 LFOS synthesis and analysis

LFOS was synthesized by incubating 5 U per mL enzyme with 0.5 M sucrose in 50 mM potassium phosphate buffer (pH 6.5) at 37 °C for 24 h. After incubation, aliquots of the reaction mixtures were taken for high-performance size-exclusion chromatography (HPSEC) and high-performance anion-exchange chromatography with pulsed amperometric detection (HPAEC-PAD) analyses. HPSEC was carried out on a Shimadzu HPLC system equipped with a refractive index detector (RID). Separation was conducted using an OHpak SB-805 HQ column (8 mm × 300 mm, Shodex) with deionized water as the eluent at a constant flow rate of 1.0 mL min^{-1}, while the column temperature was maintained at 40 °C. The molecular weight of levan was determined from a calibration curve generated using pullulan standards. HPAEC-PAD was performed on a CarboPac PA100 column (4 mm × 250 mm, Thermo Scientific). Elution was achieved using a linear gradient of sodium acetate (0–500 mM) in 150 mM NaOH for 35 min, followed by an isocratic phase at 500 mM sodium acetate in 150 mM NaOH for an additional 5 min. The separation was carried out at a flow rate of 1.0 mL min^{-1} with the column temperature set to 30 °C.

The remaining reaction mixture was mixed with equal volumes of acetone to precipitate the levan polymer, which was harvested by centrifugation at 10 000 × *g*. The isolated levan was subsequently hydrolyzed in 1 M HCl at 95 °C for 2 h. Completion of hydrolysis was confirmed by thin-layer chromatography (TLC) using Silica Gel 60 F254 plates (Merck) and a mobile phase consisting of acetic acid/acetonitrile/1-butanol/water (1 : 2:1 : 1, v/v/v/v). The amount of levan was determined from the concentration of fructose released upon acid hydrolysis using the DNS method. The concentrations of glucose, fructose, and sucrose in the reaction mixtures were quantified by HPAEC-PAD. The amount of LFOS was calculated as (moles of initial sucrose) – (moles of remaining sucrose) – (moles of free fructose) – (moles of fructose released from levan hydrolysis).

2.6 Affinity gel electrophoresis

To prepare the levan polyacrylamide gel, 0.08% (w/v) of levan was mixed with 8% non-denaturing polyacrylamide gel. A constant current of 20 mA per gel was used to run the gel at 4 °C under non-denaturing conditions in Tris-glycine buffer (25 mM Tris, 192 mM glycine, pH 8). A negative control was employed using bovine serum albumin (BSA).

2.7 Computational analysis

The crystal structure of wild-type *Et*Lsc (PDB ID: 6FRW) was obtained from the Protein Data Bank, and structural models of all *Et*Lsc variants were generated using SWISS-MODEL[18] with 6FRW as the template. The protonation states of ionizable residues at pH 6.5 were assigned through the H++ server.[19] Molecular dynamics (MD) simulations were performed with Amber20 (ref. 20) following protocols adapted from previous studies.[14] Briefly, each enzyme model was embedded in a truncated-octahedral TIP3P water box with a 13 Å solvent buffer and neutralized using Na^+ counterions. After energy minimization using procedures reported earlier, the systems were slowly heated from 0 K to the 310 K over 200 ps under NVT conditions with backbone restraints of 10 kcal $mol^{-1}\cdot Å^{-2}$. This step was followed by a 300 ps equilibration phase at the same temperatures. Production runs of 150 ns were carried out under NPT conditions (1 atm; 310 K) using the PMEMD engine, a 2 fs timestep with SHAKE algorithm,[21] and Langevin dynamics (collision frequency of 1 ps^{-1}) for temperature control.[22] Structural analyses, including calculations of root-mean-square deviation (RMSD) and root-mean-square fluctuation (RMSF), were performed using the CPPTRAJ module in Amber20.[23]

2.8 Biopurification of LFOS by yeast treatment

Residual monosaccharides in the LFOS product mixture were eliminated by treatment with yeast cells.[24] One loop of *Komagataella phaffii* (formerly known as *Pichia pastoris*) strain KM71 cells was inoculated into 20 mL of YPD medium and incubated at 30 °C, 250 rpm for 48 h. Subsequently, 2 mL of the culture was transferred into 200 mL of fresh YPD medium and incubated under the same conditions for 24 h. Cells were harvested by centrifugation at 8000 × *g* at 4 °C for 10 min. The collected yeast cells were then resuspended in 100 mL of crude LFOS product obtained from the R377A variant and incubated at 30 °C with shaking at 250 rpm for 24 h.

2.9 Prebiotic activity

Bacterial strains, including *E. coli* ATCC 25922, *Lacticaseibacillus rhamnosus* ATCC7469, *Limosilactobacillus fermentum* TISTR055, *Lacticaseibacillus casei* TISTR1463, *Lactococcus lactis* TISTR055, and *Bacillus subtilis* 168 were cultured overnight in MRS medium supplemented with 2% (w/v) glucose. The OD600 of each culture was then measured and adjusted to 0.6 using fresh MRS medium. Aliquots (10 μL) of the adjusted cultures were inoculated into 200 μL of MRS medium supplemented with sterile water (control), 1% (w/v) glucose, 1% (w/v) inulin, or 1% (w/v) LFOS in a 96-well microplate. Bacterial growth was monitored by measuring OD600 using a Synergy™ H1 microplate reader (BioTek), with orbital shaking at 37 °C. The plate was shaken at 282 cpm and paused every 10 min for OD600 measurement.

3. Results and discussion

3.1 Selection of target residue

The crystal structure of the *Et*Lsc/levanbiose complex was previously reported.[15] This provided valuable information about the amino acid residues involved in levanbiose binding. Since levanbiose is an intermediate en route to

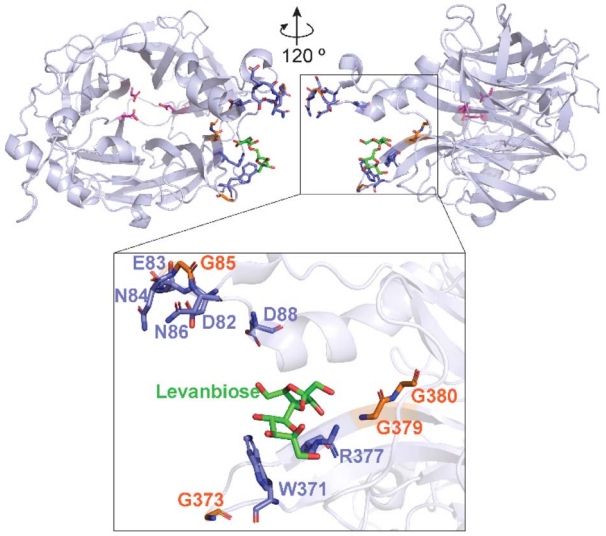

Fig. 1 Structure of *Et*Lsc/levanbiose complex (PDB ID: 6RV5) and target amino acid residue for mutagenesis. Levanbiose (green) binds at the pocket formed by loop I (residues 80–87) and loop II (residues 366–380). Amino acid residues selected for mutagenesis are highlighted as sticks, where glycine residues are shown in orange and other residues in purple.

fructooligosaccharides during the synthesis of longer-chain FOSs and levan, mutagenesis in this region may enable the enzyme to produce different sizes and yields of levan type fructooligosaccharides (LFOSs) compared to the wild-type enzyme. The levanbiose binding site is formed by two loops, namely loop I (residues 80–87) and loop II (residues 366–380). Results from molecular dynamics (MD) simulations revealed that these two loops exhibit high flexibility compared to other regions of the enzyme, suggesting that they may contribute to levan polymer binding *via* an induced-fit mechanism, where the binding site undergoes a conformational rearrangement to accommodate the incoming levan acceptor molecule.

In this study, residues located around the levanbiose binding site, including D82, E83, N84, G85, N86, D88, W371, G373, R377, G379, and G380, were selected for mutagenesis (Fig. 1). Among them, residues D82, E83, N84, N86, D88, W371, and R377 were selected because their side chains face toward levanbiose and may be directly involved in its binding; these residues were substituted with alanine. In contrast, residues G85, G373, G379, and G380 are unlikely to be directly involved in levan binding because they lack side chains, but they may contribute to protein folding and flexibility. These residues were replaced with proline to increase the rigidity of this region.

3.2 Activity and levan production rate

Variant enzymes were successfully expressed in *E. coli* and purified. Enzyme activity assays revealed that D82A and G379P exhibited significantly lower specific activities compared to the wild-type enzyme, retaining only 50% and 15% of the wild-type activity, respectively. In contrast, no detectable sucrase activity was observed for the G380P variant (Fig. 2A). Substitution of glycine to proline might impact on the folding of the protein, which may explain why the G379P and G380P mutations strongly decrease enzyme activity.

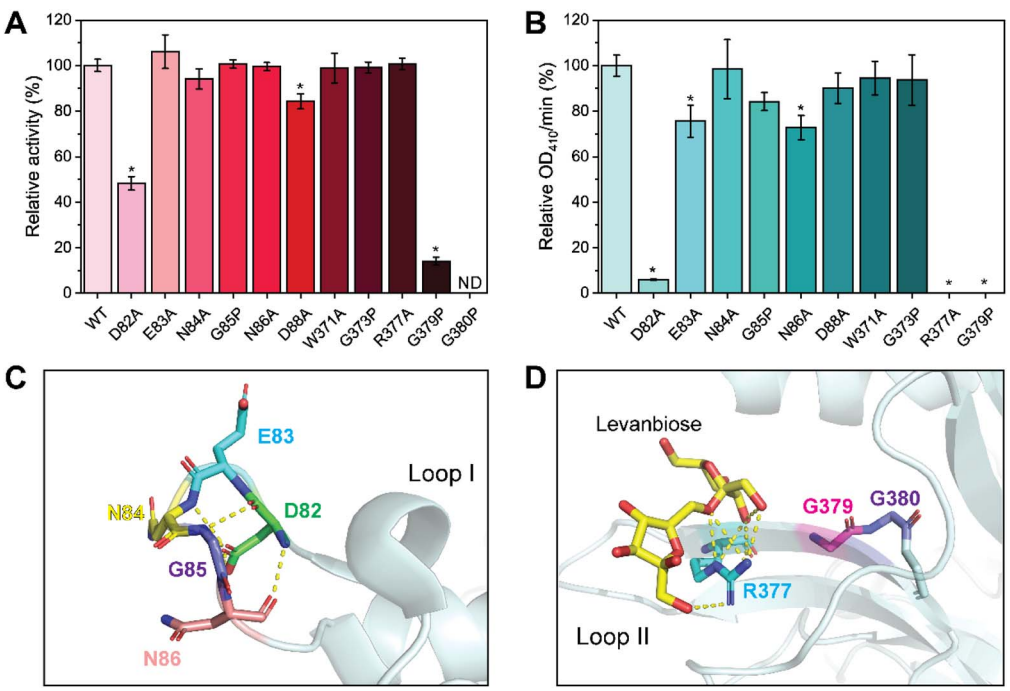

Fig. 2 Effect of mutations on enzyme activity and levan production rate. (A) Relative activity of the wild-type and variant *Et*Lsc enzymes; ND, not detected. (B) Levan production rate expressed as OD410 per min. (C) Hydrogen-bond network formed by D82 with neighboring residues in Loop I. (D) Hydrogen-bond interaction between R377 and levanbiose in Loop II. For bar graphs, data are presented as mean ± SD. Asterisks (*) in panels (A) and (B) indicate values that are significantly different from the WT. ND = not detected.

Subsequently, all variant enzymes, except G380P, were used for levan synthesis. The levan production rate was monitored by measuring the increase in turbidity (OD410) over time[25] (Fig. 2B). The results showed that the E83A and N86A mutations slightly decreased the levan production rate, whereas D82A, R377A, and G379P almost completely inhibited levan formation. Structural analysis revealed that D82 forms a hydrogen-bond network with neighboring residues within loop I, which may influence loop stability (Fig. 2C). In addition, R377 forms a hydrogen bond with levanbiose in the crystal structure (Fig. 2D). Therefore, mutations at this position and nearby residue G379 are likely to impair levan binding during polymer synthesis.

3.3 Characterization of product profile

Levan and LFOS synthesized by WT and variant *Et*Lsc were analyzed by HPSEC-RID and HPAEC-PAD. HPSEC results revealed that most variants synthesize levan of comparable molecular weight to the one produced by the WT (approximately of 2 MDa), except for the D82A, R377A, and G379P variants, in which no levan peak was detected (Fig. 3A). HPAEC-PAD analysis further demonstrated that these variants produced distinct oligosaccharide profiles compared to WT. D82A primarily produced shorter-chain LFOS, whereas R377A and G379P generated a broader distribution of oligosaccharides compared to WT (Fig. 3B). This finding suggests that R377A and G379P possess potential for LFOS synthesis, as they were unable to synthesize polysaccharide, while efficiently generating LFOS.

Subsequently, the yields of levan and LFOS were quantified. As shown in Fig. 4, WT *Et*Lsc converted approximately 7.9% of the sucrose substrate into LFOS, corresponding to 16.7% of the total transfructosylation products. In contrast, the R377A and G379P variants primarily produced LFOS, accounting for 35% and 24% of the initial sucrose, or 81.9% and 85.8% of the total transfructosylation products, respectively. The net amounts of LFOS synthesized by WT, R377A, and G379P were 6.4 g L^{-1}, 28.4 g L^{-1}, and 19.4 g L^{-1}, respectively. However, the LFOS yield

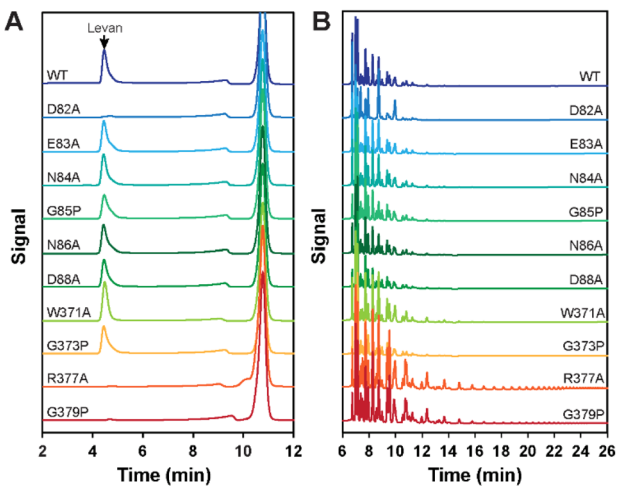

Fig. 3 Analysis of product profile using (A) HPSEC-RID and (B) HPAEC-PAD.

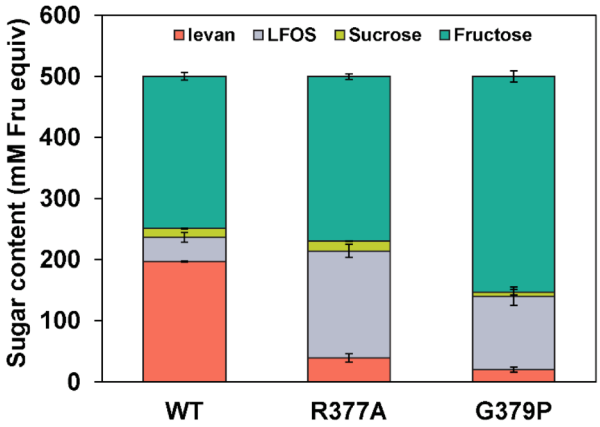

Fig. 4 The product specificity of wild-type and variant *Et*Lsc. The reactions contained 0.5 M sucrose and 5 U per mL of the enzymes in 50 mM potassium phosphate buffer (pH 6.5) at 37 °C for 24 h. Data are presented as mean ± SD.

strongly depends on the reaction conditions, such as sucrose concentration, temperature, and reaction time, which require further optimization to achieve levels suitable for industrial relevance.

In addition, the R377A variant produced a comparable amount of fructose (the hydrolysis product) compared to that of the WT, whereas G379P generated a higher level of fructose. The enhancement in LFOS yield without an additional increase in fructose formation suggests the biotechnological potential of R377A, as most fructansucrase variants that favor oligosaccharide synthesis typically exhibit higher hydrolytic activity than that of WT. For example, the N252D variant of *Priestia megaterium* levansucrase, which produces a relatively higher amount of FOS than the WT, also generates more fructose.[26] Similarly, the Y237S variant of levansucrase from *B. amyloliquefaciens* KK9 synthesized LFOS and levan only about 20% of the initial sucrose, whereas the wild-type enzyme produced approximately 40%.[12] In addition, the N251A, K372A, and R369A variants of levansucrase from *B. licheniformis* 8-37-0-1 exhibited hydrolytic activities exceeding 80%, compared with approximately 30% for the wild-type enzyme.[27] Likewise, the R483A variant of inulosucrase synthesized a higher amount of inulin-type FOSs than the WT but also produced more fructose.[5,28]

3.4 Affinity gel electrophoresis

Levan affinity PAGE was used to determine interaction between variant enzymes and levan (Fig. 5). The result clearly shows that both the R377A and G379P mutations affect the mobility shift of the enzyme molecules in the levan gel. The migration distances of these variant enzymes in the levan-containing gel were comparable to those in the gel without levan, indicating that neither enzyme interacted with levan. This behavior differs from the previously reported F376A mutation,[14] in which the variant enzyme still retained partial levan-binding ability. This finding suggests that R377 and G379 play critical roles in levan binding, consistent with the previously reported co-crystal structure of *Et*Lsc with levanbiose. The mutation of these

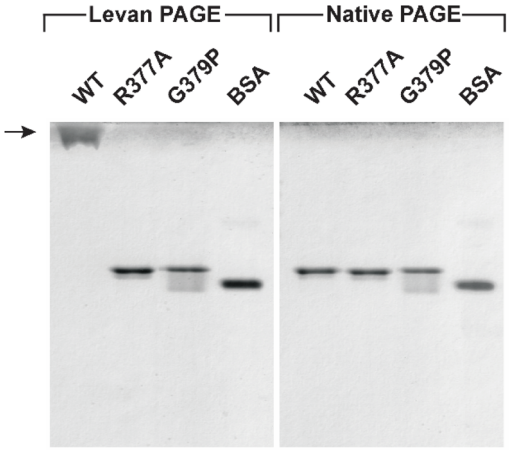

Fig. 5 Determination of levan affinity. Affinity gel electrophoresis analysis was performed using an 8% non-denaturing polyacrylamide gel containing 0.08% (w/v) levan (Levan PAGE) or without levan (Native PAGE). The mobility shift of the protein bands indicates their relative binding affinity to levan. BSA was used as a negative control.

residues would disrupt the interaction between the enzyme and the levan acceptor, suggesting why the R377A and G379P variants are incapable of synthesizing long-chain levan.

3.5 Enzyme kinetic study

Kinetic parameters of WT and variant *Et*Lsc were evaluated using sucrose as a substrate. Since *Et*Lsc could either hydrolyse sucrose or catalyse transfructosylation reactions, mutation at the levanbiose binding site might affect the enzymes mode of action. As shown in Table 1, the catalytic efficiency (k_{cat}/K_m) of the hydrolytic activity (V^F) of the R377A variant markedly increased compared with that of the WT, whereas the catalytic efficiency of its transfructosylation activity (V^{G-F}) was much lower than that of the WT. These results indicate that the R377A mutation changes the enzyme's preference toward hydrolysis while reducing its transfructosylation capability. The reduced transfructosylation efficiency of R377A suggests that the loss of the positively charged arginine residue disrupts interactions with the fructosyl acceptor or levan chain. As a result, the enzyme favors the hydrolytic pathway rather than elongating the fructan polymer.

For G379P, the catalytic efficiency of both hydrolytic (V^F) and transfructosylation activity (V^{G-F}) were notably lower than those of WT. The simultaneous reduction in both hydrolytic and transfructosylation activities indicates that the introduction of proline at this position negatively affects the overall catalytic turnover. Residue G379 is located near R377, a key levan-binding site (Fig. 2D), and this mutation likely influences the conformational dynamics of the loop in this region, which is critical for the catalytic function of *Et*Lsc.

3.6 Computational analysis

MD simulation was performed to illustrate the impact of R377A and G379P mutation on the levan synthesis efficiency of *Et*Lsc. The simulations were performed at 310 K for 150 ns, and the stability of the systems was monitored by RMSD. As shown in Fig. 6A, the RMSD of the WT and R377A *Et*Lsc stabilized within the first 40 ns of the trajectory, whereas that of the G379P variant gradually increased and reached equilibrium after approximately 100 ns. This result suggests that the G379P mutant enzyme required structural rearrangement before attaining a more energetically favorable conformation.

As a result, the MD trajectories from 130 to 150 ns were selected for further RMSF analysis. The RMSF profiles revealed that the overall structural flexibility of G379P was comparable to that of the WT enzyme, particularly around the mutated residue (Fig. 6B). This observation opposes the initial hypothesis that proline substitution would reduce the flexibility of the *Et*Lsc molecule, especially within loop II (residues 366–380). The difference is probably due to this loop changing conformation into a non-native structure, affected by the structural restriction of the proline residue. Structural analysis from the MD simulations showed that the loop II region of the WT and R377A *Et*Lsc remained stable throughout the 150 ns trajectory, whereas the corresponding region in G379P adopted an altered conformation. This structural change markedly affected the orientation of residue R377, which serves as a key levan-binding site (Fig. 6C), thereby supporting the experimental results that the G379P variant exhibited reduced activity and levan synthesis.

Table 1 Apparent kinetic constants of wild-type and mutant *Et*Lsc. Total (V^G) and transglycosylation activities (V^{G-F}) were fitted with Michaelis–Menten, while hydrolysis activity (V^F) fitted with substrate inhibition[a]

		Kinetic parameter			
*Et*Lsc		K_m (mM)	k_{cat} (s^{-1})	k_{cat}/K_m (mM^{-1} s^{-1})	K_i (mM)
WT	V^G	76 ± 5	621 ± 12	8.2	
	V^F	115 ± 61	350 ± 114	3.0	530 ± 352
	V^{G-F}	117 ± 18	461 ± 23	3.9	
R377A	V^G	83 ± 9	619 ± 20	7.5	
	V^F	23 ± 7	320 ± 35	13.6	1531 ± 730
	V^{G-F}	1513 ± 785	1227 ± 482	0.8	
G379P	V^G	367 ± 57	83 ± 6	0.2	
	V^F	509 ± 215	47 ± 11	0.1	ND
	V^{G-F}	295 ± 128	39 ± 8	0.1	

[a] ND = Not detected.

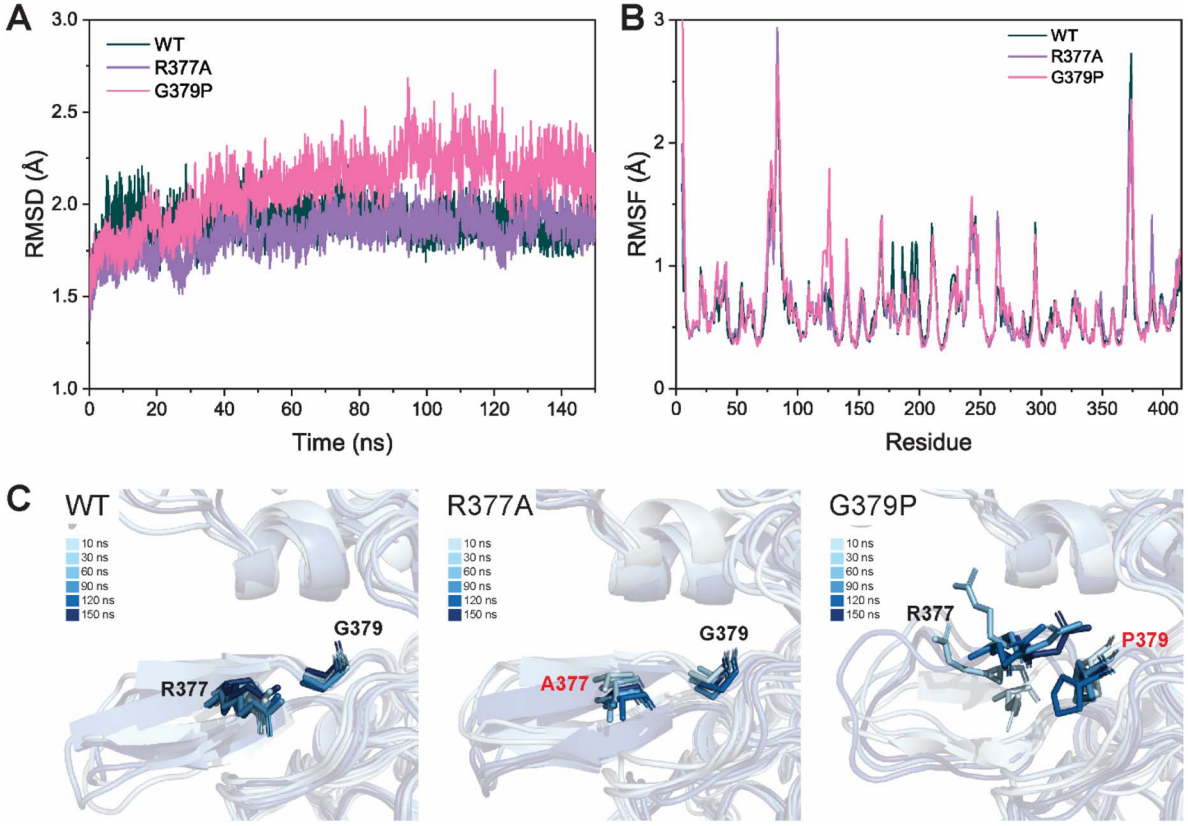

Fig. 6 Molecular dynamics simulation analysis of WT and G379P variant *Et*Lsc. (A) RMSD plots of WT, R377P and G379P during 150 ns MD simulations. (B) RMSF plot of individual residue in WT and variant *Et*Lsc analyzed from last 20 ns of MD simulation. (C) Superimposed MD snapshots (10–150 ns) illustrating that G379P alters the conformation of loop II and the orientation of residue R377.

In comparison with previous levansucrase engineering studies, residues whose mutation affected the size of the levan product were typically located near the catalytic site, such as, N251 of B. licheniformis levansucrase (approximately 7.0 Å from the closest catalytic residue),[11] Y237 of *B. amyloliquefaciens* (12.1 Å),[12] and H327 of *Brenneria sp.* (2.9 Å).[29] Mutations at these

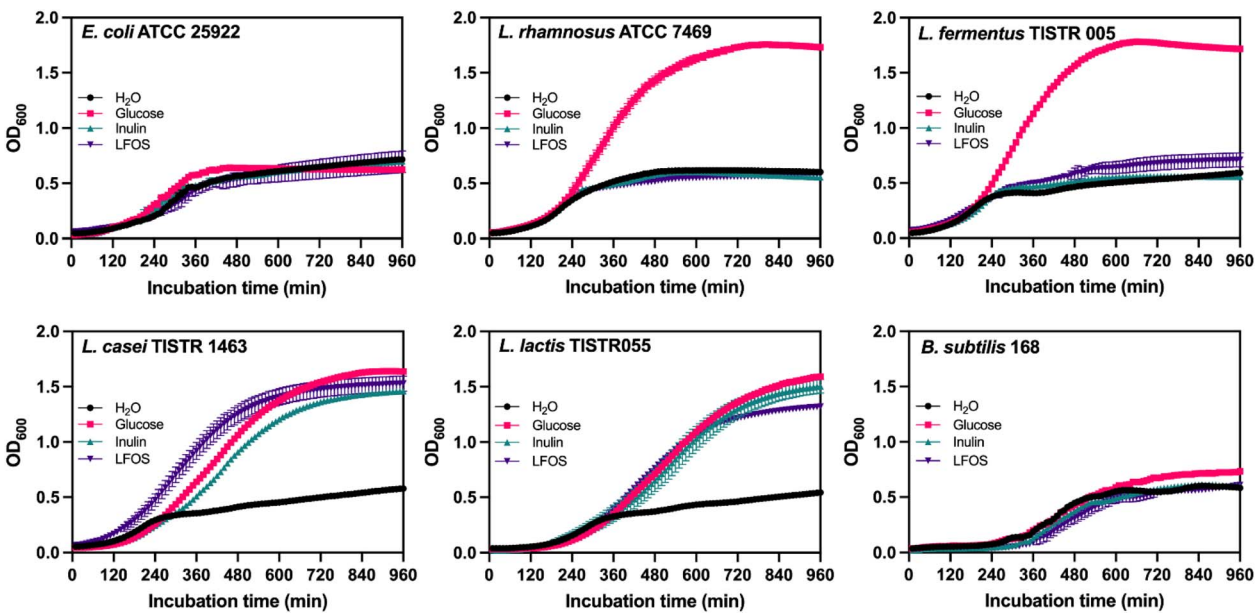

Fig. 7 Growth profiles of probiotic bacteria and *E. coli* cultured with LFOS produced by the R377A variant. Bacterial growth was monitored by measuring OD600 in media supplemented with 1% (w/v) inulin, 1% (w/v) LFOS, or without carbohydrate (control). (Data represents mean ± SD ($n = 3$).

positions generally resulted in the production of short-chain LFOS. In contrast, residue R377 is located much farther from the catalytic site of *Et*Lsc (approximately 19 Å), leading to the production of a broader molecular weight distribution of LFOS by the R377A variant. Structural alignment indicated that residue R377 in *Et*Lsc corresponds to R377 in levansucrases from *E. amylovora* (EaLsc), R399 in *Brenneria sp*. (BreLsc), R370 in Z. mobilis (ZmLsc), and R393 in *P. syringae* (PsLsc), suggesting that this position is conserved among levansucrases from Gram-negative bacteria. However, no residue equivalent to R377 in *Et*Lsc is observed when compared with levansucrases from *Bacillus* (Fig S2). This finding is consistent with previous studies reporting that the levan-binding track differs between Gram-positive and Gram-negative levansucrases.[14]

3.7 Prebiotic activity of LFOS from variant *Et*Lsc

The prebiotic activity of LFOS synthesized by the R377A variant was assessed based on the growth profiles of probiotic bacteria (*Lacticaseibacillus rhamnosus* ATCC7469, *Limosilactobacillus fermentum* TISTR055, *Lacticaseibacillus casei* TISTR1463, *Lactococcus lactis* TISTR055, and *Bacillus subtilis* 168) and *E. coli* (Fig. 7). Prior to this analysis, crude LFOS was treated with *K. phaffii* KM71 cells to remove monosaccharides. The results showed that the growth of *E. coli*, *L. rhamnosus* and *B. subtilis* in the presence of LFOS was comparable to both the inulin-treated and untreated control groups. In contrast, LFOS significantly promoted the growth of *L. fermentus*, *L. casei*, and *L. lactis*, where *L. fermentus* and *L. casei* strains exhibited higher growth on LFOS than on inulin. These results indicate that LFOS synthesized by engineered levansucrase acts as an effective prebiotic, selectively stimulating the growth of specific probiotic bacteria without promoting the growth of a pathogenic strain. The probiotic growth-promoting effect observed in this study is consistent with recent reports demonstrating that levan-based and inulin-based fructans enhance the growth of *L. paracasei*, a species phylogenetically closely related to the probiotic strains examined herein.[30,31] Previous studies have suggested that the stimulatory effect of LFOS on probiotic bacteria is attributable to their ability to metabolize levan-type fructooligosaccharides as a carbon source.[30] In this context, the present results further support the potential of LFOS as a functional prebiotic ingredient, highlighting its relevance for applications in food biochemistry and functional food development.

4. Conclusions

This study demonstrates that engineering the levanbiose-binding site of *E. tasmaniensis* levansucrase provides an efficient approach for modulating product specificity. Mutations at residues R377 and G379 blocked levan polymerization while significantly enhancing LFOS formation, yielding up to 82–86% LFOS of total transfructosylation products. Also, the activity of the R377A variant is comparable to that of the wild-type enzyme. A prebiotic activity assay revealed that the LFOS produced by R377A stimulates the growth of probiotic strains, including *L. fermentus*, *L. casei* and *L. lactis*. Altogether, these findings provide mechanistic insights into levan elongation in Gram-negative levansucrases and demonstrate R377 as a key engineering hotspot for the high-yield production of bioactive LFOSs.

Conflicts of interest

There are no conflicts to declare.

Data availability

The data that support the findings of this study are available from the corresponding author (T. C.) upon reasonable request.

Supplementary information (SI): oligonucleotide primers for mutagenesis, enzyme kinetic curves, and structural alignments. See DOI: https://doi.org/10.1039/d5ra10086k.

Acknowledgements

This project is funded by National Research Council of Thailand (NRCT): Contract number N42A670836. We would like to thank Department of Biochemistry, Faculty of Science, Chulalongkorn University, Thailand; and Department of Chemistry, Faculty of Science, Silpakorn University, Thailand for the use of experimental and computational facilities.

References

1 P. Singh, S. K. Gupta, A. Kundu, M. Grover and S. Saha, *Food Biosci.*, 2025, **63**, 105726.
2 Y. Wang, T. Zeng, S.-e. Wang, W. Wang, Q. Wang and H.-X. Yu, *Nutrition*, 2010, **26**, 305–311.
3 G. S. Dias, A. C. Vieira, G. Baioni e Silva, N. F. Simões, T. S. Milessi, L. S. Saraiva, M. D. Xavier, A. A. Longati, M. F. Rodrigues, S. Fernandes, E. S. Silva, A. E. Maiorano, S. A. Morales, R. C. Basso and R. F. Perna, *Processes*, 2025, **13**(4), 1252.
4 S. Singh and S. Gaur, in. *Valorization of biomass to bioproducts*, ed. V. K. Gupta, Elsevier, 2023, pp. 71–85, DOI: 10.1016/B978-0-12-822887-6.00001-2.
5 T. Charoenwongpaiboon, T. Sitthiyotha, P. P. Na Ayutthaya, K. Wangpaiboon, S. Chunsrivirot, M. Hengsakul Prousoontorn and R. Pichyangkura, *Carbohydr. Polym.*, 2019, **209**, 111–121.
6 T. Charoenwongpaiboon, K. Wangpaiboon, P. Septham, N. Jiamvoraphong, S. Issaragrisil, R. Pichyangkura and C. Lorthongpanich, *Int. J. Biol. Macromol.*, 2022, **221**, 1121–1129.
7 R. Srikanth, G. Siddartha, C. H. S. S. Sundhar Reddy, B. S. Harish, M. Janaki Ramaiah and K. B. Uppuluri, *Carbohydr. Polym.*, 2015, **123**, 8–16.
8 T. Charoenwongpaiboon, C. Charoenwongphaibun, K. Wangpaiboon, P. Panpetch, N. Wanichacheva and R. Pichyangkura, *Int. J. Biol. Macromol.*, 2024, **271**, 132508.
9 T. Charoenwongpaiboon, K. Wangpaiboon, P. Panpetch and R. Pichyangkur, *Sci. Asia*, 2025, 51.

10 K. Wangpaiboon, M. Klaewkla, T. Charoenwongpaiboon, N. Vongkusolkit, P. Panpetch, K. Kuttiyawong, W. Visessanguan and R. Pichyangkura, *Enzyme Microb. Technol.*, 2022, **154**, 109960.
11 P. Kanjanatanin, R. Pichyangkura, T. Sitthiyotha, T. Charoenwongpaiboon, K. Wangpaiboon and S. Chunsrivirot, *Int. J. Biol. Macromol.*, 2019, **140**, 1239–1248.
12 P. Phengnoi, T. Charoenwongpaiboon, K. Wangpaiboon, M. Klaewkla, S. Nakapong, W. Visessanguan, K. Ito, R. Pichyangkura and K. Kuttiyawong, *Biomolecules*, 2020, **10**(5), 692.
13 X. Zhang, W. Xu, D. Ni, W. Zhang, C. Guang and W. Mu, *J. Agric. Food Chem.*, 2023, **71**, 680–689.
14 T. Charoenwongpaiboon, S. Benini, R. A. Field, M. Klaewkla, C. Lorthongpanich, P. Pongsawasdi, R. Pichyangkura and K. Wangpaiboon, *Carbohydr. Polym.*, 2026, **373**, 124616.
15 I. Polsinelli, R. Caliandro, N. Demitri and S. Benini, *Int. J. Mol. Sci.*, 2020, **21**(1), 83.
16 K. L. Heckman and L. R. Pease, *Nat. Protoc.*, 2007, **2**, 924–932.
17 G. L. Miller, *Anal. Chem.*, 1959, **31**, 426–428.
18 A. Waterhouse, M. Bertoni, S. Bienert, G. Studer, G. Tauriello, R. Gumienny, F. T. Heer, T. A. P. de Beer, C. Rempfer, L. Bordoli, R. Lepore and T. Schwede, *Nucleic Acids Res.*, 2018, **46**, W296–W303.
19 R. Anandakrishnan, B. Aguilar and A. V. Onufriev, *Nucleic Acids Res.*, 2012, **40**, W537–W541.
20 D. A. Case, H. M. Aktulga, K. Belfon, D. S. Cerutti, G. A. Cisneros, V. W. D. Cruzeiro, N. Forouzesh, T. J. Giese, A. W. Götz, H. Gohlke, S. Izadi, K. Kasavajhala, M. C. Kaymak, E. King, T. Kurtzman, T.-S. Lee, P. Li, J. Liu, T. Luchko, R. Luo, M. Manathunga, M. R. Machado, H. M. Nguyen, K. A. O'Hearn, A. V. Onufriev, F. Pan, S. Pantano, R. Qi, A. Rahnamoun, A. Risheh, S. Schott-Verdugo, A. Shajan, J. Swails, J. Wang, H. Wei, X. Wu, Y. Wu, S. Zhang, S. Zhao, Q. Zhu, T. E. Cheatham III, D. R. Roe, A. Roitberg, C. Simmerling, D. M. York, M. C. Nagan and K. M. Merz Jr., *J. Chem. Inf. Model.*, 2023, **63**, 6183–6191.
21 J.-P. Ryckaert, G. Ciccotti and H. J. C. Berendsen, *J. Comput. Phys.*, 1977, **23**, 327–341.
22 X. Wu and B. R. Brooks, *Chem. Phys. Lett.*, 2003, **381**, 512–518.
23 D. R. Roe and T. E. Cheatham III, *J. Chem. Theory Comput.*, 2013, **9**, 3084–3095.
24 Y.-l. Yang, J.-h. Wang, D. Teng and F. Zhang, *J. Agric. Food Chem.*, 2008, **56**, 2805–2809.
25 T. Charoenwongpaiboon, K. Wangpaiboon, R. Pichyangkura and K. Kuttiyawong, *ACS Omega*, 2025, **10**(46), 55592–55599.
26 A. Homann, R. Biedendieck, S. Götze, D. Jahn and J. Seibel, *Biochem. J.*, 2007, **407**, 189–198.
27 C. He, Y. Yang, R. Zhao, J. Qu, L. Jin, L. Lu, L. Xu and M. Xiao, *Appl. Microbiol. Biotechnol.*, 2018, **102**, 3217–3228.
28 T. Charoenwongpaiboon, M. Klaewkla, S. Chunsrivirot, K. Wangpaiboon, R. Pichyangkura, R. A. Field and M. H. Prousoontorn, *RSC Adv.*, 2019, **9**, 14957–14965.
29 W. Xu, D. Ni, X. Hou, T. Pijning, A. Guskov, Y. Rao and W. Mu, *J. Agric. Food Chem.*, 2022, **70**, 5095–5105.
30 J. C. Pohlentz, N. Gallala, K. Kosciow and M. Hövels, *J. Funct.Foods*, 2022, **99**, 105343.
31 D. Konkol, M. Kuźmińska-Bajor, J. P. Madej, E. Popiela, M. Lis, M. Kuczkowski, M. Szczypka, K. Sierżant, M. U. Ashgar, K. Leicht, M. Korzeniowska, C. Ceccopieri and M. Korczyński, *Anim. Feed Sci. Technol.*, 2025, **330**, 116529.